

Microphase separation of diblock copolymer poly(styrene-*b*-isoprene): A dissipative particle dynamics simulation study

Xuejin Li, Jiayi Guo, Yuan Liu, and Haojun Liang^{a)}

Department of Polymer Science and Engineering and Hefei National Laboratory for Physical Sciences at Microscale, University of Science and Technology of China, Hefei, Anhui 230026, People's Republic of China

(Received 16 October 2008; accepted 2 January 2009; published online 20 February 2009)

Dissipative particle dynamics (DPD) simulations have been employed to study the microphase separation of the poly(styrene-*b*-isoprene) (PS-*b*-PI) diblock copolymer. The DPD model is constructed to match the physical description and structural properties of the PS-*b*-PI diblock copolymer. A coarse-grained force field has been developed for the diblock copolymer system in DPD simulations. The new force field contains bonded and nonbonded interaction terms, which are derived from atomistic molecular dynamics simulations and determined by fitting experimental data of the compressibility of water at room temperature and interfacial tension values, respectively. The morphologies of the PS-*b*-PI diblock copolymer system obtained from DPD simulations are in agreement with experimental observations as well as previous simulated results. © 2009 American Institute of Physics. [DOI: 10.1063/1.3077865]

I. INTRODUCTION

Block copolymers are a special type of polymer in which each molecule consists of two or more chemically distinct blocks that are covalently linked together. They are further classified by the number of blocks each molecule contains, and how they are arranged. Owing to the repulsive interactions among the different blocks and the topological constraints caused by the subchains being linked permanently, block copolymers represent an interesting class of polymer materials that exhibit a rich variety of phase behaviors in bulk and concentrated solutions, making them a subject of great interest for experiments,¹⁻⁴ theories,⁵⁻⁸ and computer simulations.⁹⁻¹⁶ Diblock copolymers are the simplest case of block copolymer in which only two distinct chemical blocks are involved (an *A*-block and a *B*-block). Typically, the polymers or blocks that make up diblock copolymers are immiscible and ideal for phase separation. Compared to a complete separation of the binary mixtures into a single *A*-rich domain and a single *B*-rich domain, the existing chemical bonds between two blocks in diblock copolymers make complete separation impossible. As a consequence, microphase separation occurs, resulting in complex morphologies, such as spherical, cylindrical, and lamellar microstructures.

In order to develop skills to control the sizes and shapes of microstructures, an understanding of the formation of these microstructures under different conditions is required. With increasing computer power, computer simulations have become the main pillars of scientific research and have become powerful tools for investigating various phenomena in complex systems, such as block copolymers. Presently, however, the quantitative modeling of block copolymer chains in full atomistic detail at meso- or macroscopic length scales

remains difficult because of the huge number of degrees of freedom in such system. A potential solution to overcome this problem is to reduce the number of degrees of freedom through the mapping of an atomistic model onto coarse-grained (CG) structures. Actually, there has been a growing interest in developing CG models for diblock copolymers chains.^{12,15,17-30} Here, we briefly describe a few of the major achievements. Groot and Madden¹² studied the microphase separation of linear diblock copolymer melts by dissipative particle dynamics (DPD) simulation method. Recently, the microphase separations of nonlinear diblock copolymers have been investigated using a similar method.^{21,25,31} The phase behaviors of diblock copolymers by the off-lattice Monte Carlo simulation have been studied by Besold *et al.*¹⁷ Ginzburg *et al.*¹⁸ developed a new CG model for diblock copolymers to investigate the influence of nanoscale particles on the phase separation and the morphologies of symmetric diblock copolymer films. In a recent series of papers, Addison *et al.*¹⁹ proposed a model of systematic CG representation of block copolymer by modeling the chain as two soft blobs tethered by an entropic spring. Pierleoni *et al.*²⁴ studied the self-assembly of diblock copolymer through a two-step CG strategy to build blocks of supermolecular structures. Sambriski and Guenza²⁷ described a similar method for CG diblock copolymer liquids based on the solution of liquid-state integral equations. To our knowledge, few studies have looked into the phase structures of specific diblock copolymers. The morphologies and mechanical properties of poly(styrene-*b*-isoprene) (PS-*b*-PI) diblock copolymers have recently been studied by Soto-Figueroa *et al.*^{22,32-34} Ortiz *et al.*²³ developed a DPD model of diblock copolymer similar to ours, inasmuch as the optimization of the CG force field is obtained by incorporating the bonded interaction parameters from atomistic simulations and nonbonded interaction parameters from experimental data. In our previous

^{a)}Author to whom correspondence should be addressed. Electronic mail: hjiang@ustc.edu.cn.

simulations, we have developed a CG force field for the PS-*b*-PB diblock copolymer.¹⁵ In this present work, we have further developed our approach to address this problem of modeling of diblock copolymer.

II. SIMULATION DETAILS

A. DPD formulation

DPD is a mesoscopic simulation method, introduced in 1992 by Hoogerbrugge and Koelman.³⁵ In a DPD simulation, a particle represents the center of mass of a cluster of atoms and the mass, length, and time scales are all unity. Particles i and j interact with each other via a pairwise additive force, consisting of three contributions: (i) a conservative force, F_{ij}^C ; (ii) a dissipative force, F_{ij}^D ; and (iii) a random force, F_{ij}^R . Hence, the total force on particle i is given by

$$F_i = \sum_{i \neq j} F_{ij}^C + F_{ij}^D + F_{ij}^R, \quad (1)$$

where the sum acts over all particles within a cutoff radius r_c . Specifically, in our simulation,

$$F_i = \sum_{i \neq j} a_{ij} \omega(r_{ij}) \hat{r}_{ij} - \gamma \omega^2(r_{ij}) (\hat{r}_{ij} \cdot \mathbf{v}_{ij}) \hat{r}_{ij} + \sigma \omega(r_{ij}) \zeta_{ij} \Delta t^{-1/2} \hat{r}_{ij}, \quad (2)$$

where a_{ij} is a maximum repulsion between particles i and j ; r_{ij} is the distance between them, with the corresponding unit vector \hat{r}_{ij} ; \mathbf{v}_{ij} is the difference between the two velocities; ζ_{ij} is a random number with zero mean and unit variance; and γ and σ are parameters coupled by $\sigma^2 = 2\gamma k_B T$. The weighting function $\omega(r_{ij})$ is given by

$$\omega(r_{ij}) = \begin{cases} 1 - \frac{r_{ij}}{r_c}, & r_{ij} < r_c, \\ 0, & r_{ij} \geq r_c. \end{cases} \quad (3)$$

By joining consecutive particles with spring force, one can construct CG models of polymers.^{12,36} The harmonic spring force with a spring constant of k_s and an equilibrium bond length of r_s in our simulations has the form

$$F_{ij}^S = k_s (1 - r_{ij}/r_s) \hat{r}_{ij}. \quad (4)$$

B. Force field of diblock copolymer

Atomistic force fields of diblock copolymers are usually divided into two major parts,³⁷ namely, bonded and non-bonded potential terms, each of which comprises several different contributors. The total force field energy can be described as

$$V_{\text{tot}} = V_{\text{bonded}} + V_{\text{nonbonded}} = (V_{\text{str}} + V_{\text{bend}} + V_{\text{tors}} + (V_{\text{vdw}} + V_{\text{es}} + \dots)), \quad (5)$$

where V_{tot} is the total energy of the system; V_{str} and V_{bend} are the potentials defining the contributions for bond stretching between pairs of bonded atoms and the angular bending among three atoms, respectively; V_{tors} is a torsional potential accounting for the change of energy as bonds rotate; V_{vdw}

accounts for the excluded volume repulsive and intermolecular attractive forces between atoms in different copolymer chains or in the same copolymer chains, but at least three bonds apart; and V_{es} is the potential of the electrostatic interactions. The CG force field for the diblock copolymer in DPD simulations is built similarly using these two potential terms, that is, V_{bonded} and $V_{\text{nonbonded}}$. Specifically, the bonded interactions in the DPD scheme are described by the harmonic spring force, as stated in Eq. (4), and bond-bending force, which has the form

$$F^\theta = -\nabla V_{\text{bend}}, \quad (6)$$

$$V_{\text{bend}} = \frac{1}{2} k_\theta (\theta - \theta_0)^2, \quad (7)$$

where k_θ and θ_0 are the bending constant and equilibrium angle between two consecutive bonds, respectively. The non-bonded interactions are represented by the pairwise additive forces. Specifically, these interaction terms are described by the conserved parts of the forces since the DPD system has the correct Boltzmann distribution. According to our previous simulations,¹⁵ all of these interaction terms are not intended to make adjustments simultaneously but to perform successive adjustment of these terms in the order of their relative strength, as expressed by

$$F_{ij}^S \rightarrow F^\theta \rightarrow F_{ij}^C. \quad (8)$$

We choose to begin with the harmonic spring forces and work our way systematically down to the conservative forces.

C. DPD model construction

For a DPD simulation of the block copolymer system and for the specific case of the PS-*b*-PI diblock copolymer system, the choice of the CG procedure for the DPD particles and the optimization of the CG force field for the DPD model are of fundamental importance.

1. Mapping

Within the DPD approach, some molecules of the system are CG by a set of particles with a necessary assumption that each particle has the same volume based on the CG mapping on that of water, that is, the amount of matter contained in each particle is constant for all species. To construct the DPD model for the PS-*b*-PI system, we first need to figure out the volume of simulated monomers and process the CG mapping for PS and PI. The volume of a molecule is calculated by a method somewhat similar to the Monte Carlo method, that is, by measuring how many vertices of a dense regular grid happen to be within the probe radius of the molecule's atoms. Specifically, it is calculated using a modified version of the program named MOL_VOLUME developed by Balaeff.³⁸ The values of monomer volumes are listed in Table I. From these parameters, we find the ratio of the volume of PS monomer and PI monomer to that of water molecule to be 5.33 and 4.52, respectively. As a rough approximation, the volume of one PS (or PI) monomer is considered to be the same as that of five molecules of water. Therefore, within a standard mapping of five molecules of water per DPD par-

TABLE I. Parameters of monomer volume and interfacial tension of PS with PI in our simulations. The experiment measured interfacial tension at temperature $T=413$ K is obtained from Ref. 41.

Molecule	Volume V (\AA^3)	Interfacial tension σ (mN/m)
Water	29.9	...
Styrene	159.4	1.68 ± 0.02
Isoprene	135.3	

article, we use the conventional coarse-graining strategy of approximately one PS (or PI) monomer per DPD particle. Figure 1 illustrates the mapping of the PS and PI monomers from the atomistic to mesoscopic level. Each monomer is replaced by one DPD particle located at the center of the mass and connected by harmonic springs.

2. Length, time, and temperature scales

In the DPD approach, it is convenient to use reduced units.^{36,39} The unit of length is defined by the cutoff radius r_c ; the unit of the mass is defined by the masses of particles; and the unit of energy is defined by $k_B T$. Here, we will give an estimate of the physical length, time, and temperature scales in our DPD simulations. Since the simulated particle number density is $\rho r_c^3 = 3$ and a DPD particle has the volume of approximately 150 \AA^3 , a cube that contains three particles therefore corresponds to a volume of approximately 450 \AA^3 ; thus, we find the physical length scale of interaction radius by

$$r_c = \sqrt[3]{450} = 7.66 \text{ \AA}. \quad (9)$$

Following Groot and Rabone,³⁹ since the value of the number of waterlike molecules per DPD particle has been chosen at $N_m = 5$, the time scale is estimated by

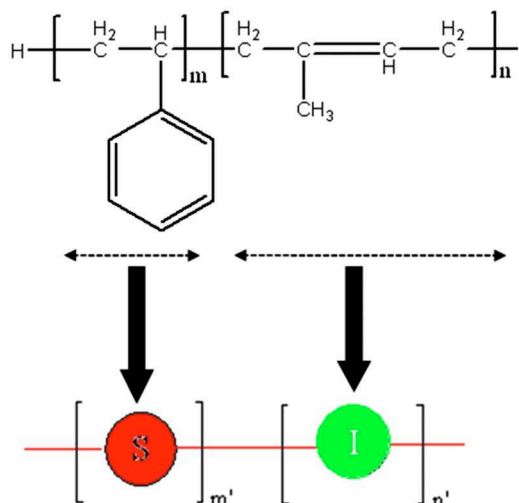


FIG. 1. (Color online) Illustration of the CG mapping of PS-*b*-PI diblock copolymer from atomistic to DPD model. In the figure, the S and I particles represent the PS and PI monomers, respectively.

$$\tau = \frac{N_m D_{\text{sim}} R_c^2}{D_{\text{water}}} = 7.89 \pm 0.1 N_m^{5/3} = 115.9 \pm 0.1 \text{ ps}. \quad (10)$$

In our simulations, a constant time step of $\Delta t = 0.01 \tau$ is used, thus, the time step of $\Delta t = 1.16 \text{ ps}$ is taken in the simulations.

Since the mass, length, and energy are all unity within the DPD approach, the temperature is expressed in reduced units as well. To use reduced units, we define $k_B T_0 = 1.0$, where T_0 is room temperature. The repulsive interactions can then be expressed in these reduced units, that is, the repulsive parameters of waterlike particles have been fitted to give the correct compressibility of water at room temperature. Then, we introduce a notation T^* to indicate the reduced temperature. In order to estimate the values of reduced temperatures in terms of physical temperatures, we have mapped the reduced temperatures, T^* , onto physical temperatures T , according to the following linear equation:

$$T = aT^* + b. \quad (11)$$

The values of coefficients are found by solving the system of linear equations obtained by substituting, in Eq. (11), the reduced and physical values of absolute zero and room temperatures, 0 and 298.15 K, respectively. The resulting values are $a = 298.15 \text{ K}$ and $b = 0 \text{ K}$.

3. Bonded interactions

The bonded interactions in the DPD scheme are described by harmonic spring forces between consecutive particles and bond-bending forces between consecutive bonds. The equilibrium values and the force constants in DPD simulations are derived from all-atom molecular dynamics (AAMD) simulation. First, an AAMD simulation of PS-*b*-PI is performed in the NVT ensemble with the temperature set to $T = 413 \text{ K}$. The distributions of distances between two successive particles and the distributions of angles between two consecutive bonds along the chains can then be obtained from the simulation. The equilibrium values and the force constants in DPD simulations are chosen to reproduce the obtained means and standard deviation of the target bond length and bend angle distributions. According to our previous simulations,¹⁵ since two different types of DPD particles have been chosen in the DPD model, three different types of bond distributions and four different angle distributions are used to describe the bonded interactions. Table II summarizes the parameters of bonded interactions in the DPD simulations.

4. Nonbonded interactions

The nonbonded interactions in the DPD scheme are described by the repulsion parameters related to the interactions between DPD particles. The value of repulsion parameter for waterlike particles is chosen such that the simulated compressibility of waterlike particles at room temperature corresponds to the experimental value. Generally, it has been previously proposed that the following equation should hold in a DPD system:³⁹

TABLE II. The developing of the interaction parameters from atomistic simulation to DPD scheme.

Interactions	AAMD Simulation		DPD simulation	
Bonded terms				
	k_s	r_0	k'_s $\left(\frac{m_w k_B T}{R_c^2}\right)$	r'_0 (R_c)
Bond length	$(k_B T)$	(nm)		
S-S	1.14	0.602	3.717	0.786
S-I	22.06	0.488	71.889	0.637
I-I	13.79	0.470	44.946	0.614
	k_θ	θ_0	k'_θ $\left(\frac{m_w k_B T}{\text{rad}^2}\right)$	θ'_0 (rad)
Bend angle	$(1/\text{rad}^2)$	(deg)		
S-S-S	2.33	88.6	0.466	1.546
S-S-I	11.12	71.0	0.617	1.240
S-I-I	5.68	138.6	0.315	2.419
I-I-I	1.31	125.1	0.073	2.184
Nonbonded terms				
Repulsive force			S	I
S			131.5	140.5
I			140.5	131.5

$$\frac{1}{k_B T} \left(\frac{\partial P}{\partial \rho} \right)_{\text{sim}} = \frac{N_m}{k_B T} \left(\frac{\partial P}{\partial n} \right)_{\text{exp}}, \quad (12)$$

where ρ and n are the particle density of the DPD system and the density of waterlike molecules in waterlike liquid, respectively. In Sec. II C the value of the number of waterlike molecules per DPD particle has been chosen at $N_m=5$. For this value, the correct compressibility of waterlike particle at room temperature is matched when the repulsion parameter of waterlike particle is determined at $a_{ii}=131.5k_B T$. Note that the same values are taken between particles of the same type for all liquid components because we actually simulate equal liquid volumes for all components. In principle, this procedure may be applied at any temperature, and may thus result in temperature-dependent a_{ij} -repulsive parameters; however, it will make the interpretation of the simulation data too difficult when dealing with temperature-dependent parameters. Therefore, we make an approximation in which we assume that the a_{ij} -repulsive parameters are not temperature dependent. Considering the fact that a direct mapping between the atomistic-level information and the repulsive parameters in a DPD model is not always possible, the value of parameters referring to the interaction between two different particles is determined by fitting the values of experimental interfacial tension.⁴⁰ To obtain the simulated interfacial tension values, a DPD system consisting of PS-*b*-PI bilayer is simulated in a periodic box, where the bilayer is oriented perpendicular to the x -axis, and the interfacial tension is determined by integrating the difference between normal and tangential stress across the interface separating the two segregated components via the formula

$$\begin{aligned} \sigma_{\text{DPD}} &= \int [P_{xx}(x) - 0.5(P_{yy}(x) + P_{zz}(x))] dx \\ &= \frac{1}{A} \sum_{i < j} (F_{ij,x} x_{ij} - 0.5(F_{ij,y} y_{ij} + F_{ij,z} z_{ij})), \end{aligned} \quad (13)$$

the quality interfacial tension is then obtained,

$$\sigma_{\text{calc}} = \frac{k_B T}{R_c^2} \sigma_{\text{DPD}}, \quad (14)$$

which can be directly compared to experimentally measured interfacial tension. From the simulations, we find that the simulated value of interfacial tension at the repulsive parameter $a_{ij}=140.5k_B T$ has a very close approximation to the experimental interfacial tension value of approximately 1.68 mN/m at $T=413$ K.⁴¹ Therefore, we have chosen the value $a_{ij}=140.5k_B T$ in the succeeding simulations.

D. Computational details

All of the simulations are carried out in a simulation box of $20 \times 20 \times 20$ containing a total of 24 000 constituent particles with a particle number density of 3 at $T^*=1.386$. The simulations are performed using a modified version of the DPD code named MYDPD.^{42,43} The time integration of motion equations is done using a modified velocity-Verlet algorithm with $\lambda=0.65$ and time step $\Delta t=0.01$. The number of representative particles for each PS-*b*-PI diblock copolymer chain is assumed to be constant. In our simulations, the diblock copolymer length is $N=10$ and the first fN particles are of type S particles where the parameter f is denoted as the ratio of the length of the S-block relative to the whole block copolymer, and the last $(1-f)N$ are of type I particles. We initialize our system by distributing PS-*b*-PI diblock copolymer chains randomly in the simulation box; therefore, the final microstructures can be considered as dependent of the composition and initial architecture of the diblock copolymer. A series of simulations is presented to study the microphase structures of PS-*b*-PI by varying the parameter f , that is, the fraction of S particles in the system, from 0.10 to 0.90.

III. RESULTS AND DISCUSSIONS

In this section, we present the simulated results of the PS-*b*-PI diblock copolymer system. We start our simulations from a symmetric diblock copolymer consisting of S and I blocks of equal length, that is, $f=0.50$. Owing to the symmetry of the diblock copolymer, the lamellar structure is expected. In the simulation, it is observed that the S_5I_5 block system converges to a lamellar phase, as shown in Fig. 2(a). When we change the composition of the diblock copolymer from symmetric to asymmetric, other microstructures appear, which are also shown in Fig. 2. When the fraction of the S-block decreases from $f=0.50$, the lamellar phase disappears and the gyroid microstructure is first observed by interconnection of microdomains of the same component, and the hexagonal packed cylinder (hex) morphology is then observed when the composition of the diblock copolymer is more asymmetric. Upon further decrease of the fraction of the S-block, the PS-*b*-PI diblock copolymer displays spheri-

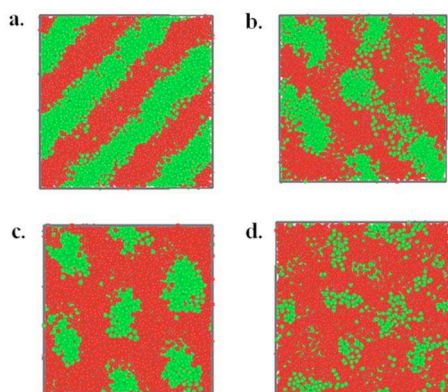


FIG. 2. (Color online) Morphologies of the PS-*b*-PI diblock copolymer system obtained from the DPD simulations: (a) lamellar (LAM), (b) gyroid, (c) hexagonal packed cylinder (HEX), and (d) body-centered cubic (BCC) microstructures.

cal morphology formed by body-centered-cubic (bcc) packing of the S-blocks into the matrix of the I-blocks. Finally, the system is disordered upon further decreasing of the fraction f . Upon increasing the S-block fraction, the morphology appears in a reversed order and asymmetric systems evolve again. The simulated morphologies appear in the same order with expectation based on experiments and theories, that is, the phase transitions from disordered to bcc to hex to gyroid to lamellar microstructures are in line with experimental results and theoretical simulations. To visualize the three-dimensional structure of this phase more clearly, the density of S-blocks is measured on a three-dimensional grid. In the S-rich domains, the density is high and in the I-rich domains, it is low. The dividing surface between the S-rich domains and the I-rich domains is represented by the isosurface where the density is midway between these values. Figure 3 shows the simulated morphologies of PS-*b*-PI diblock copolymer systems and their composition domains, which are similar to the simulated results by Soto-Figueroa *et al.*²² However, the CG procedure for the DPD particles and the optimization of the CG force field for the DPD model are different. First, the DPD particles for the PS-*b*-PI in their model were obtained

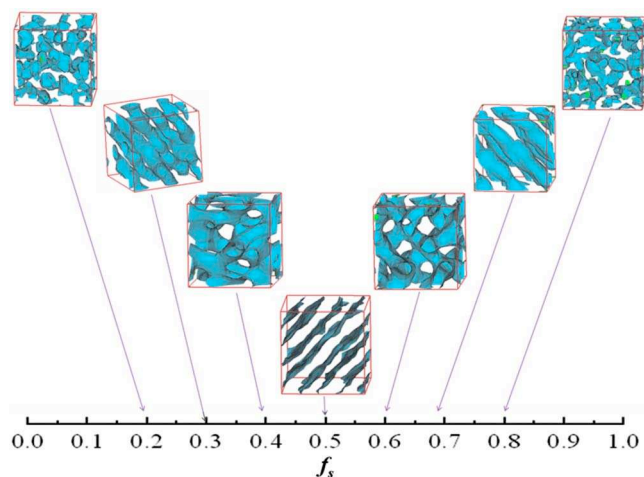


FIG. 3. (Color online) Simulated morphologies for PS-*b*-PI diblock copolymer systems obtained from the DPD simulations and their composition domains.

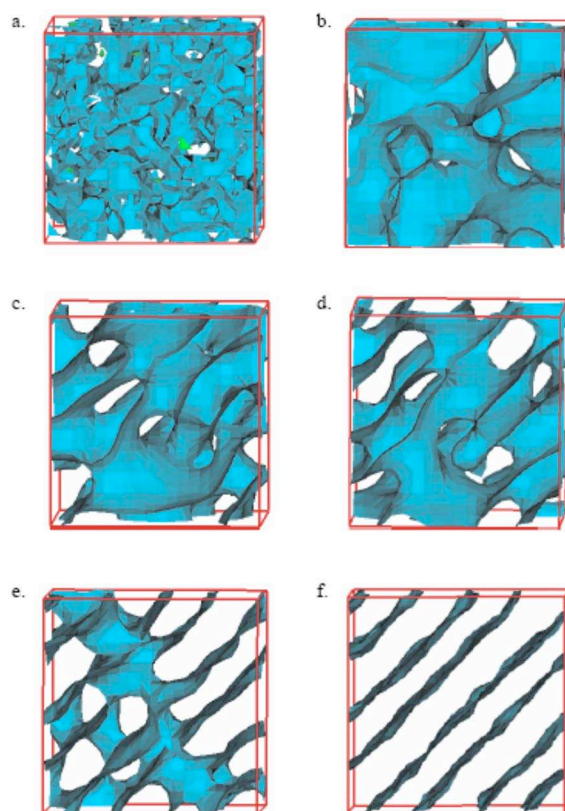


FIG. 4. (Color online) Sequential snapshots of the formation of lamellar morphology from the PS-*b*-PI diblock copolymer system at t equals (a) $0.006 \mu\text{s}$, (b) $0.12 \mu\text{s}$, (c) $0.17 \mu\text{s}$, (d) $0.29 \mu\text{s}$, (e) $0.58 \mu\text{s}$, and (f) $0.70 \mu\text{s}$.

from the molecular structures of the copolymer chains based on a standard Gaussian model; whereas the CG procedure in our DPD model is derived from the standard DPD approach that keeps each DPD particle with the same volume based on the CG mapping on that of water. Second, the repulsive interactions of DPD particles in their model were obtained from the monomer-monomer interactions; however, in our DPD scheme, these repulsive parameters are determined by fitting experimental data for interfacial tension and compressibility of water. In addition, the bonded interactions in our DPD model, which are described by harmonic spring forces and bond-bending forces, are derived from atomistic molecular dynamic simulations. The appearance of similar morphologies from two different DPD schemes for PS-*b*-PI suggests that the computational modeling is robust against details of the methods.

A direct observation of the dynamic processes for the formation of these complex microstructures is important for developing skills to control the sizes and shapes of these microstructures. The simulation provides a good choice to understand these processes. A typical dynamic formation process of lamellar microstructure is provided in Fig. 4. The process of this microstructure can be clearly understood from these figures. It reveals that the block copolymers initially rapidly aggregate into localized spherical and cylindrical microstructures [Fig. 4(a)]. Then these microstructures come into close contact and form gyroid morphology [Fig. 4(b)]. Next, an irregular hexagonal cylindrical morphology

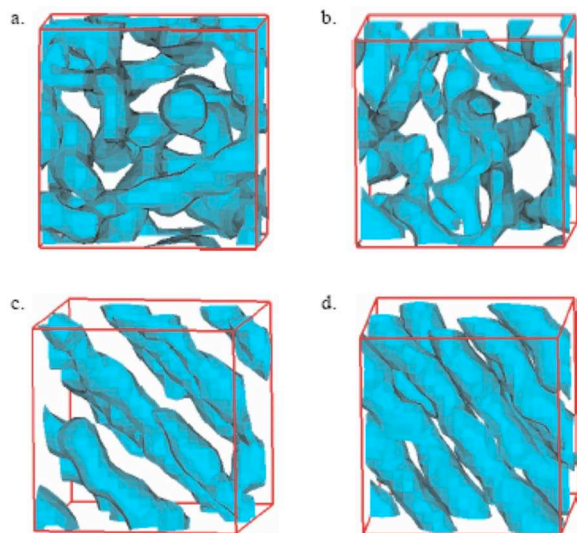


FIG. 5. (Color online) Sequential snapshots of the formation of hexagonal packed cylindrical morphology from the PS-*b*-PI diblock copolymer system at t equals (a) 0.12 μ s, (b) 1.16 μ s, (c) 1.97 μ s, and (d) 2.32 μ s.

[Fig. 4(c)] appears. This morphology subsequently evolves first, into a perforated hexagonal lamellar morphology [Fig. 4(d)], and second, into an irregular lamellar morphology [Fig. 4(e)] in which some microdomains between two alternating layers are connected. The observations of the perforated hexagonal and irregular lamellar morphology are in agreement with the experimental results reported by Mani *et al.*⁴⁴ and recently simulated results reported by Soto-Figueroa *et al.*³³ Finally, the connections between two alternating layers are broken and the lamellar microstructure appears [see Fig. 4(f)].

Decreasing the fraction of the S-block from $f = 0.50$ – 0.40 , gyroid morphology is observed. Once this microstructure forms, it remains stable in this study. The dynamic pathway of hexagonal packed cylinders obtained during the microphase evolution process is presented in Fig. 5. This process also initiates the formation of spherical and cylindrical microstructures, and then the gyroid morphology [Fig. 5(a)]. Irregular cylindrical microstructure [Fig. 5(b)] is then formed, in which the cylinders tend to be arranged in a parallel manner. Next, the cylinders are completely aligned [Fig. 5(c)], although some sideward microdomains are still connected. Finally, the sideward connections are broken and the hexagonal packed cylindrical morphology appears [see Fig. 5(d)]. The bcc morphology can be directly evolved from the spherical and cylindrical microstructures after a much larger time scale; however, this morphology is slightly different from the bcc morphology observed via theory and experiment. This morphology observed in our simulation is not exactly of cubic symmetry, and the microstructures of small micelles are more like peanut shapes than ideal spheroids. The existing difference can be explained by the fact that the finite length of diblock copolymers and the finite size of the simulation box. In our DPD model, the simulated diblock copolymers are only of length $N=10$. The finite polymer length can have a great effect on the phase diagram, through it is not of the highest importance to estimate the interfacial tension, as described by Groot and Madden.¹² An-

other reason for the existing difference may be the finite size of the simulation box. The bcc phase has to fit the simulation box in three directions and the limited box size forces the system to change the shapes of micelles.

The dynamics of these morphologies are similar to that reported by Groot and Madden,¹² where they proposed a direct, a particle-based DPD model without any real molecular structure of the block copolymers. In this work, we study the morphologies of the PS-*b*-PI diblock copolymer system at a constant temperature $T=413$ K. The DPD model is constructed to match the physical description and structural properties of the PS-*b*-PI diblock copolymer. The parameters of CG force field are developed from AAMD simulation and experimental data. Within the new CG force field, a run of more than 2.0×10^6 iterations (2.32 μ s) is required to obtain some of the equilibrium morphologies, such as the hex and bcc morphologies, which are much greater than the time used in the previous DPD simulation.

IV. CONCLUSION

This paper describes the DPD simulation results of the PS-*b*-PI diblock copolymer. The DPD model is constructed to match the physical description and structural properties of the PS-*b*-PI diblock copolymer system. The CG procedure for the DPD particles is derived from the standard DPD approach that keeps each DPD particle with the same volume based on the CG mapping on that of water. A CG force field is developed for the PS-*b*-PI diblock copolymer system in DPD simulations. The new DPD force field includes two interaction parts, the bonded and nonbonded interactions. The bonded interactions in the DPD scheme are described by harmonic spring forces and bond-bending forces, which are derived from AAMD simulation for the PS-*b*-PI diblock copolymer. The nonbonded interactions in the DPD scheme are determined by fitting experimental data for the compressibility of water at room temperature and interfacial tension values. The morphologies obtained from our DPD simulation for the PS-*b*-PI diblock copolymer systems can be compared qualitatively with expectation based on experiments, theories, and other simulation results. Although we develop the DPD model only for PS-*b*-PI, the approach should be compatible for use with other diblock copolymer systems and other polymer systems in general.

ACKNOWLEDGMENTS

We are grateful for the financial support provided by the Outstanding Youth Fund (No. 20525416), the Program of the National Natural Science Foundation of China (Nos. 20874094 and 50773072), and the NBRPC (No. 2005CB623800). Parts of the simulations were carried out at the Shanghai Supercomputer Center.

¹F. S. Bates and G. H. Fredrickson, *Annu. Rev. Phys. Chem.* **41**, 525 (1990).

²A. K. Khandpur, S. Forster, F. S. Bates, I. W. Hamley, A. J. Ryan, W. Bras, K. Almdal, and K. Mortensen, *Macromolecules* **28**, 8796 (1995).

³G. H. Fredrickson and F. S. Bates, *Annu. Rev. Mater. Sci.* **26**, 501 (1996).

⁴M. F. Schulz, A. K. Khandpur, F. S. Bates, K. Almdal, K. Mortensen, D. A. Hajduk, and S. M. Gruner, *Macromolecules* **29**, 2857 (1996).

- ⁵G. H. Fredrickson and E. Helfand, *J. Chem. Phys.* **87**, 697 (1987).
- ⁶M. W. Matsen and F. S. Bates, *Macromolecules* **29**, 1091 (1996).
- ⁷M. W. Matsen and F. S. Bates, *Macromolecules* **29**, 7641 (1996).
- ⁸M. W. Matsen and F. S. Bates, *J. Polym. Sci., Part B: Polym. Phys.* **35**, 945 (1997).
- ⁹K. Binder and H. Fried, *Macromolecules* **26**, 6878 (1993).
- ¹⁰A. Hoffmann, J. U. Sommer, and A. Blumen, *J. Chem. Phys.* **106**, 6709 (1997).
- ¹¹A. Hoffmann, J. U. Sommer, and A. Blumen, *J. Chem. Phys.* **107**, 7559 (1997).
- ¹²R. D. Groot and T. J. Madden, *J. Chem. Phys.* **108**, 8713 (1998).
- ¹³A. J. Schultz, C. K. Hall, and J. Genzer, *J. Chem. Phys.* **117**, 10329 (2002).
- ¹⁴M. A. Horsch, Z. L. Zhang, C. R. Iacovella, and S. C. Glotzer, *J. Chem. Phys.* **121**, 11455 (2004).
- ¹⁵X. J. Li, D. Z. Kou, S. L. Rao, and H. J. Liang, *J. Chem. Phys.* **124**, 204909 (2006).
- ¹⁶D. Bedrov, C. Ayyagari, and G. D. Smith, *J. Chem. Theory Comput.* **2**, 598 (2006).
- ¹⁷G. Besold, O. Hassager, and O. G. Mouritsen, *Comput. Phys. Commun.* **121–122**, 542 (1999).
- ¹⁸V. V. Ginzburg, C. Gibbons, F. Qiu, G. W. Peng, and A. C. Balazs, *Macromolecules* **33**, 6140 (2000).
- ¹⁹C. I. Addison, J. P. Hansen, V. Krakoviack, and A. A. Louis, *Mol. Phys.* **103**, 3045 (2005).
- ²⁰M. Muller and G. D. Smith, *J. Polym. Sci., Part B: Polym. Phys.* **43**, 934 (2005).
- ²¹H. J. Qian, Z. Y. Lu, L. J. Chen, Z. S. Li, and C. C. Sun, *Macromolecules* **38**, 1395 (2005).
- ²²C. Soto-Figueroa, M. R. Rodriguez-Hidalgo, and J. M. Martinez-Magadan, *Polymer* **46**, 7485 (2005).
- ²³V. Ortiz, S. O. Nielsen, D. E. Discher, M. L. Klein, R. Lipowsky, and J. Shillcock, *J. Phys. Chem. B* **109**, 17708 (2005).
- ²⁴C. Pierleoni, C. Addison, J. P. Hansen, and V. Krakoviack, *Phys. Rev. Lett.* **96**, 128302 (2006).
- ²⁵Y. Xu, J. Feng, H. L. Liu, and Y. Hu, *Mol. Simul.* **32**, 375 (2006).
- ²⁶M. J. Cass, D. M. Heyes, and R. J. English, *Langmuir* **23**, 6576 (2007).
- ²⁷E. J. Sambriski and M. G. Guenza, *Phys. Rev. E* **76**, 051801 (2007).
- ²⁸R. Kumar and M. Muthukumar, *J. Chem. Phys.* **126**, 214902 (2007).
- ²⁹T. D. Sewell, K. O. Rasmussen, D. Bedrov, G. D. Smith, and R. B. Thompson, *J. Chem. Phys.* **127**, 144901 (2007).
- ³⁰M. G. Guenza, *J. Phys.: Condens. Matter* **20**, 033101 (2008).
- ³¹Y. Xu, J. Feng, H. L. Liu, and Y. Hu, *Mol. Simul.* **34**, 559 (2008).
- ³²C. Soto-Figueroa, L. Vicente, J. M. Martinez-Magadan, and M. R. Rodriguez-Hidalgo, *J. Phys. Chem. B* **111**, 11756 (2007).
- ³³C. Soto-Figueroa, M. R. Rodriguez-Hidalgo, J. M. Martinez-Magadan, and L. Vicente, *Macromolecules* **41**, 3297 (2008).
- ³⁴C. Soto-Figueroa, M. R. Rodriguez-Hidalgo, J. M. Martinez-Magadan, and L. Vicente, *Chem. Phys. Lett.* **460**, 507 (2008).
- ³⁵P. J. Hoogerbrugge and J. M. V. A. Koelman, *Europhys. Lett.* **19**, 155 (1992).
- ³⁶R. D. Groot and P. B. Warren, *J. Chem. Phys.* **107**, 4423 (1997).
- ³⁷A. R. Leach, *Molecular Modeling: Principles and Applications* (Prentice Hall, Harlow, 2001).
- ³⁸See: <http://www.ks.uiuc.edu/Development/MDTools/molvolume/>.
- ³⁹R. D. Groot and K. L. Rabone, *Biophys. J.* **81**, 725 (2001).
- ⁴⁰A. Maiti and S. McGrother, *J. Chem. Phys.* **120**, 1594 (2004).
- ⁴¹N. P. Adhikari and E. Straube, *Macromol. Theory Simul.* **12**, 499 (2003).
- ⁴²G. De Fabritiis, M. Serrano, P. Espanol, and P. V. Coveney, *Physica A* **361**, 429 (2006).
- ⁴³M. Serrano, G. De Fabritiis, P. Espanol, and P. V. Coveney, *Math. Comput. Simul.* **72**, 190 (2006).
- ⁴⁴S. Mani, R. A. Weiss, M. E. Cantino, L. H. Khairallah, S. F. Hahn, and C. E. Williams, *Eur. Polym. J.* **36**, 215 (2000).